Article

Discrete Element-Based Simulation Analysis and Research of Potato Soil Agglomerate Fragmentation and Separation

Dong Yan [ID]**, Weigang Deng *** [ID]**, Shengshi Xie** [ID]**, Chenglong Liu, Zhiqi Ren, Haohao Zhao, Yansong Cai and Zexin Zhao**

College of Mechanical and Electrical Engineering, Inner Mongolia Agricultural University, No. 306 Zhao Wuda Road, Hohhot 010010, China; fengye9819@163.com (D.Y.); xieshengshi@163.com (S.X.); m15395713450@163.com (C.L.); heroren970326@163.com (Z.R.); m13772562813@163.com (H.Z.); a996723415@163.com (Y.C.); m15124756760@163.com (Z.Z.)

* Correspondence: wg_deng@126.com

Abstract: To study the influence law of the overburden rotating plate mechanism on the fragmentation and separation of potato soil agglomerates, a single-factor test and a response surface test simulation analysis of the soil fragmentation process were conducted in EDEM 2022 software. The results of the single-factor test show that the triangular rack blade of the overburdened rotating plate mechanism has the best effect on soil fragmentation and separation. With the increase in the lower blade speed, the upper lift chain bar line speed, and the tilt angle of the mechanism, the effect on the fragmentation and separation of potato soil agglomerates decreases. The response surface test results show that the debris removal rate decreases with the increase in blade speed and tilt angle, the percentage of bond breakage between potato soil particles declines with the rise of blade speed and lift chain bar line speed, and the percentage of bond breakage between soil particles increases with the increase in blade speed and lift chain bar line speed. The optimal solution was obtained by using the optimization function in Design-Expert 13 software, which was adjusted as follows: the blade rack type was triangular, the lift chain bar line speed was 0.307 m/s, the blade speed was 0.4 m/s, and the tilt angle was 40°. The research methods and results provide a reference for the simulation of potato soil crushing and separation motion in a sandy loam soil cultivation area.

Keywords: overburden rotating plate; EDEM; discrete element; potato soil agglomerates; fragmentation and separation

1. Introduction

Potato is one of China's four staple foods, and as the scale of potato cultivation continues to expand, research on mechanized potato harvesting has become increasingly important. Soil crushing and separation is a crucial part of the potato harvesting process, which directly affects the efficiency of potato harvesting and damage. At present, most of the soil crushing and separation devices are in the form of lifting chains and separating sieves. Wei optimized the wavy separating sieve surface of the segmented potato harvester, constructed a soil and potato block model based on discrete elements, clarified the influence of the sieve surface structure and operating parameters on the soil crushing and separation process, and verified the rationality and feasibility of the system [1]. Wen and Sun designed and tested the conveyor belt type potato seeder and lift chain type potato excavator, respectively, and completed soil crushing and separation better without considering the size requirement of the device [2,3]. But the longer lift chain directly increased the size and power of the machine, which was primarily used in large machinery. The swing-type separation screen is widely used with small- and medium-sized harvesting machines due to its simple structure, low power consumption, and high efficiency [4]. Wang established the discrete element model of a swing sieve, potato, and soil for the swing sieve device

and completed a discrete element simulation of the soil crushing and separation process, which proved the uncertainty of the potato group effect on potato movement on the sieve surface [5]. Li optimized the design of the separating screen and designed a third-order six-boom separating screen, which can effectively complete soil crushing and separation, and analyzed the characteristics of potato movement on the separating screen [6]. However, the potatoes will be scattered on the ground after the soil crushing and separation process is completed, which increases the manual pickup labor intensity. In addition, drum-type separation devices have a more significant impact on potato damage and are less frequently used [7–9]. Compared with the previous devices, the soil crushing and separating device in this article with the overburden rotating plate can not only use the lifting chain and the overburden rotating plate to effectively complete the soil crushing and separation, but also occupy a small space, and can be applied to both the medium-sized and large-scale potato combine harvesters.

The discrete element method is a new numerical calculation method used to analyze the motion laws and mechanical characteristics of complex discrete systems [10]. It was first proposed by Peter Cundall [11] and applied to the motion analysis of rock slopes. In recent years, with the continuous improvement of discrete element theory and related software, more and more scholars have applied discrete element software to the design of agricultural machinery, simulating the working process of machinery and exploring the laws of material movement. With the rapid development of computer technology, EDEM, a numerical simulation software based on the discrete unit method, has been used in agricultural research. Huang WJ calibrated parameters for sandy soils in discrete element simulation [12]; Li used EDEM simulation to calibrate parameters for sandy soils with different moisture contents, which proved the reliability of bonding parameters and provided a parameter basis for discrete element simulation of potato soil separation [13]; and Jiang studied the shear strength of sandy loam soils based on the discrete element simulation approach [14]. Alfaris Murtadha A. A. studied the effects of lateral spacing between deep plowing and shallow plowing on the average weight diameter and soil crushing energy of deep plowing by a self-made deep plowing plow [15]. A. A. Tagar studied the effects of traditional tillage methods on soil fragmentation and aggregate stability and their relationship with fractal dimension [16]. Martinez Alexandra da Silva studied the relationship between crop rotation and soil fragmentation and examined its influence on soil penetration resistance [17]. Zhao Bangtai studied the mechanical performance analysis and test of a multi-stage digging shovel of a potato harvester [18]. Li used the Hertz–Mindlin model to study the soil around potato tubers in the field, which provided a reference for the construction of the soil model in the potato field and the discrete element simulation of harvesting devices and soil [19]. Chen studied the parameter calibration method for cassava tubers in discrete element simulation, and the physical and simulation parameters of the cassava tubers were determined, which provided a research method for the parameter calibration of the material [20]. Liu conducted a discrete element simulation study on the hemp yam root-soil complex and clayey soil in a hemp yam cultivation area and obtained the relationship between morphological indexes of four hemp yam capillary roots and the ultimate shear of hemp yam capillary root-soil complex by measuring and regression analysis of the maximum shear of hemp yam capillary root–soil complex [21,22]. Liu used the discrete element method to calibrate the parameters of the potato in the simulation, which provided data support for the discrete element simulation of the potato [23]. Liu and Zhang carried out the potato motion simulation during harvest based on the discrete element method. And the motion characteristics and collision of the potatoes were analyzed, which provided a theoretical basis for the study of potato collision damage [24,25]. Wei et al. applied the particle bonding model to potato soil separation for the first time, examining the degree of soil fragmentation and screening effect under different operating conditions [1]. Song et al. used the Hertz–Mindlin model combined with a bonding contact model to aggregate simulated mulberry soil particles through bonding. A simulated direct shear test was carried out by combining a physical test and simulation

verification to verify the reliability of the bonding parameters obtained [26]. Whereas most people study sandy loam soil, Wu et al. used the Hertz–Mindlin model to carry out simulation experiments on clay soil and obtained JKR surface energy, the coefficient of restitution, and other influence factors, as well as parameter calibration results [27]. The particle bonding model can not only be used for the fragmentation and separation of aggregates between potatoes and soil but is also widely used in discrete element simulations of other crops and particles. Tao took sugarcane cultivation soil (with a moisture content of 16.3%) in the coastal area of Guangxi as the research object and selected the Hertz–Mindlin with JKR cohesion contact model in EDEM to calibrate the discrete element simulation model parameters between soil particles, soil and trenching, and covering devices [28]. Yu established a biaxial calibration test based on the contact bonding model in the particle discrete element method. Through a large number of repeated numerical experiments, the corresponding relationship between the micro parameters and the macro parameters of the small river slope soil was obtained, providing a reference method and macro parameter correspondence for establishing soil models [29]. Fan took Guizhou clay loam soil as the research object, simulated the situation of high soil moisture content (21%) on rainy days, and used a combination of actual and simulation experiments to use the Hertz–Mindlin with bonding in EDEM as the contact model between soil and soil, as well as between soil and soil contact materials, to obtain the optimal parameter values, and verified the optimal parameter values. This provides a feasible solution for studying clay loam soil [30]. Song used a combination of experiments and simulations to obtain the physical and contact parameters of soil particles in the soil discrete element simulation model. The method used mulberry garden soil as a sample to simulate and calibrate the contact parameters of soil particles, providing reliable data and theory for the discrete element simulation analysis and structural optimization of the interaction between the soil contact components of mulberry garden tillage machinery and soil in sandy loam soil [26]. Zhang used the Hertz–Mindlin bonding contact model to establish a discrete element bonding model for banana straw and calibrated its parameters, providing a theoretical reference for the design and research of banana straw crushing and returning machines [31]. Li uses EDEM discrete element simulation software to calibrate the contact parameters between soil and soil contact materials (65 Mn) using slope tests, and the contact parameters between soil and soil are calibrated using stacking angle tests. This provides reference data for the study of soil discrete element simulation [32]. The bonded particle model is widely used to establish large particle seed models, but it is limited by modeling methods and has a more significant difference in surface roughness compared to traditional spherical filling methods. Zhang, in response to this issue, calibrated the interspecific static friction coefficient and rolling friction coefficient of the corn particle bonding model and obtained reliable data, providing a reference for the selection of calibration parameter ranges in the subsequent simulation process of pneumatic seeders [33]. At this point, the research on soil discrete elements has been relatively complete, but there is relatively little research on the aggregation of potatoes and soil. This article uses a particle bonding model to establish potato soil agglomerate models and conduct a discrete element fragmentation simulation analysis.

This article establishes different potato soil agglomerate models using particle bonding models and analyzes the influence of structural and operational parameters of the overburden rotating plate mechanism on potato soil agglomerate fragmentation. This study not only provides the basic data for the optimal design of the overburden rotating plate mechanism but also provides a reference for the design and simulation analysis of the soil breaking and separating mechanism in the harvesting process of potato and other rhizome crops.

2. Materials and Methods

2.1. Structure and Working Principle of the Soil Crushing and Separating Device

Figure 1 shows the model diagram of the potato harvester and the model diagram of the overburden rotating plate mechanism. The potato harvester is pulled forward by the

tractor, and the potato soil agglomerate is dug up by the excavator and transported to the crushing and separation device. The tractor power is transmitted to the active sprocket of the lifting chain and the rotary overburden device through the transmission mechanism, and the potato soil agglomerate is conveyed backward when the lifting chain rotates. The potato soil agglomerate is beaten by the soil-breaking blades of the rotary overburden device driven by the chain and gravity to complete the first soil breaking and shattering of the potato soil agglomerate; subsequently, the initially broken potato soil agglomerate is sandwiched between the upper rotary overburden device and the lower lift chain and lifted with the lift chain bars; the sprocket of the rotary overburden device and the lift chain sprocket set a differential speed, and the soil-breaking blades scrape over each bar to squeeze the potato soil agglomerate. Every time the soil crushing blade scrapes through a bar, the potato soil agglomerate will be crushed once and then passed from the end of the lift chain to the subsequent device.
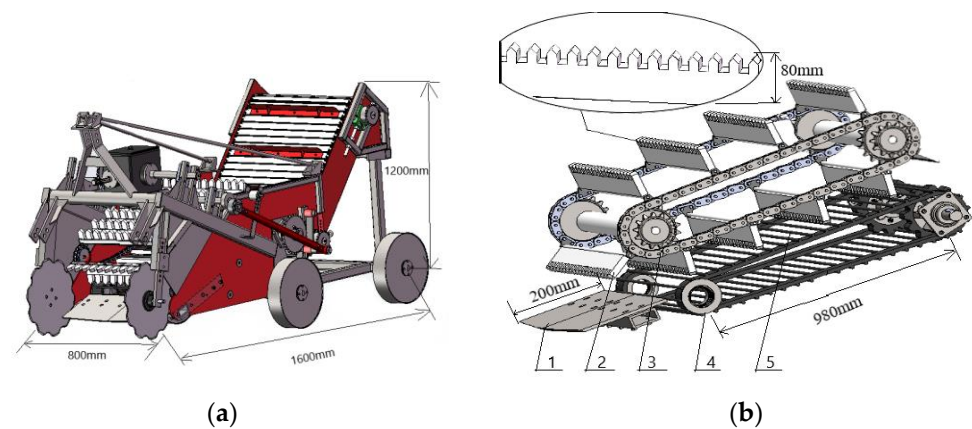

Figure 1. (**a**) Three-dimensional model of the potato harvester unit. (**b**) Three-dimensional model of the soil crushing and separating unit. 1. Excavating shovel; 2. soil crushing blade; 3. rotating shaft gear; 4. lifting chain guide wheel; 5. lifting chain bar.

2.2. Raw Materials

2.2.1. Potato Modeling

To establish the potato solid model, the 3D scanning method is usually adopted to obtain the potato three-dimensional grid model with the STL format [34]. In this article, potatoes of 0.4–0.6 kg were selected to obtain a three-dimensional model by a 3D scanning method. The scanned potato model was imported into EDEM 2022 software in STL format, and then the potato discrete element model was obtained by the particle filling method. The potato 3D scanning model and the discrete element particle filling model are shown in Figure 2.
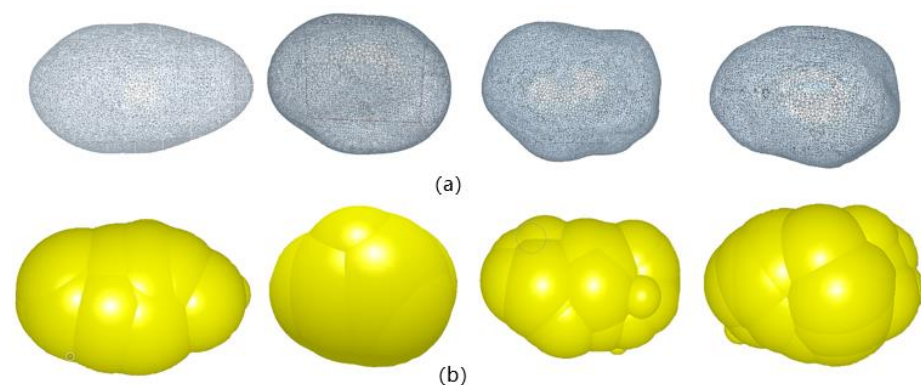

Figure 2. (**a**) Potato scanning model. (**b**) Filled model.

2.2.2. Modeling of Potato Soil Agglomerates

The soil is usually irregularly geometric during the crushing and separation process. The ground is initially excavated, wrapped around the potato in roughly long lumps, generally close to 700 mm in length and 200 mm in depth, and is transformed from large agglomerates into small, scattered clods by the transport of the lift chain and the extrusion of the overburden rotating plate mechanism before falling to the end of the lift chain. Based on the soil size distribution observed in field harvesting tests on sandy soils, the soil agglomerates broken at the end of the lift chain are simplified to soil particles with a radius of 5 mm [35].

The particle bonding model is a basic model in EDEM, and the principle is to use the ideal elastic bonding of particles to form aggregates that can be broken. The model construction process for potato soil aggregates is first to build a soil trough model in SolidWorks, then generate a certain proportion of potato particles and soil particles to fill the trough model, and finally extrude the model using a loaded plane. The filled soil particles have a physical radius of 5 mm and a contact radius of 5.5 mm. We define 0.5 mm as the threshold. We use the value of 0.5 mm as the threshold because during the actual harvesting process of the potatoes when large soil particles are broken, the smallest soil particles that break out are mostly around a radius of 0.5 mm. When the distance between the two particles exceeds the threshold of 0.5 mm, the two particles separate. When the contact distance between the two particles after compression falls below this threshold, bonds will form. The filled soil trough model has a length of 700 mm and a width of 150 mm, the load plane length and width are the same as the soil trough model, and the load value is equal to the product of the standard atmospheric pressure and the load plane area, which is 10,639 N.

The process of constructing the potato soil aggregate model in EDEM is shown in Figure 3. The yellow spheres represent soil particles and the red spheres represent potato particles. First, establish a compression filling model (soil tank model), fill the filling model with soil particles and potato particles, and then simulate the extrusion molding through EDEM. After obtaining the complete extrusion model, the Hertz–Mindlin bonding contact model in EDEM was used to introduce parallel bonding bonds between spherical particles in the polymer, forming a crushable potato soil aggregate for simulation, as shown in Figure 3. In the final rice grain model with adhesive bonds, the color of the particle changes from red to blue, representing the increase in bond force from small to large. The discrete element model of potato soil agglomerates is shown in Figure 4.
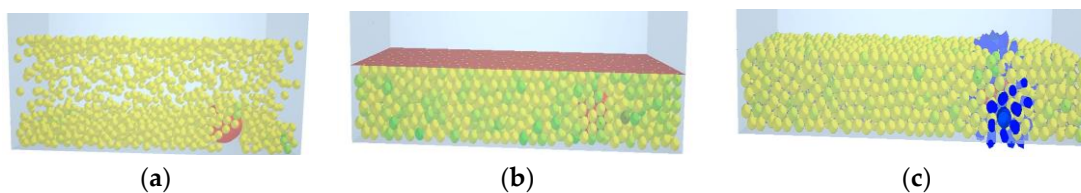

(**a**)   (**b**)   (**c**)

Figure 3. (**a**) Fill in the model. (**b**) Squeezing. (**c**) Obtaining particle agglomerates.
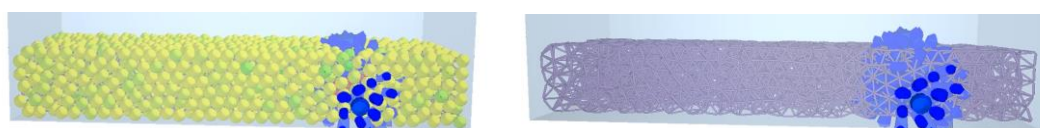

Figure 4. Discrete element model of potato soil agglomerates.

The model generated 12,732 soil particles, 4 potato particles, 2854 bonding bonds between potato and soil particles, and 5771 bonding bonds between soil particles. The final model is shown in Figure 5.
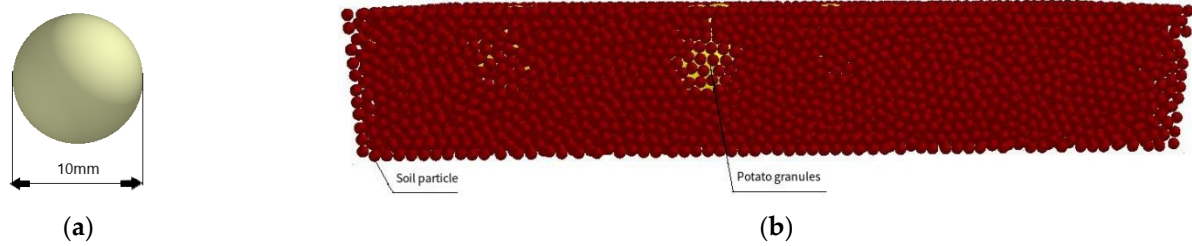
(**a**)   (**b**)

Figure 5. (**a**) Soil particle model. (**b**)Potato soil agglomerate model.

2.2.3. Soil Crushing and Separation Mechanism Modeling

The rotary overburden device shown in Figure 1b was further simplified in SolidWorks and imported into EDEM 2022 software. Rubber is used for the blade material, and 65Mn is used for the rest.

During the work process, the potato soil agglomerates moved only in the space between the lower part of the overburdened rotating plate mechanism and the upper part of the lift chain. Therefore, in the simulation environment, only the movement of the lower blades was set. The lift chain is constantly rotating circularly.

The soil crushing and separation simulation is shown in Figure 6. When the blade rotates above the potato soil aggregates, the soil is slapped due to collision. Subsequently, the difference in speed between the blade and the lifting chain drives the potato soil aggregates to move along the surface of the lifting chain toward to the end, continuously breaking and separating the bound soil particles. During this period, the bonding between particles is shown in Figure 7.
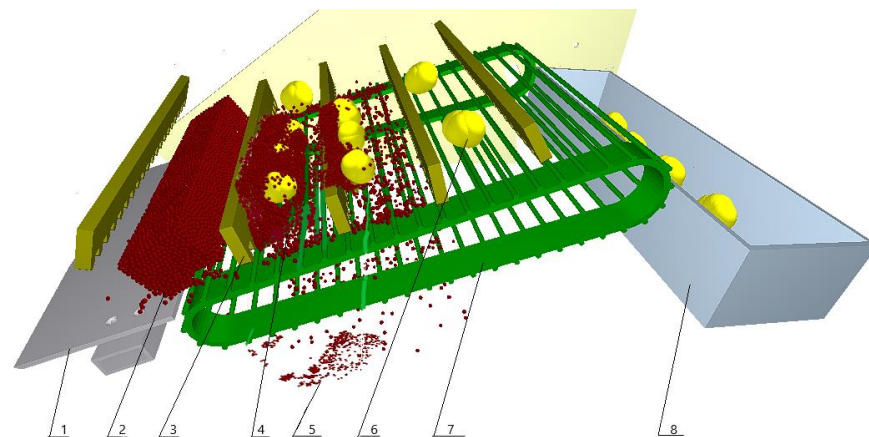

Figure 6. Simulation flowchart of the soil crushing and separation device. 1. Excavation shovel; 2. potato soil agglomerate before crushing; 3. blade for crushing soil; 4. potato soil agglomerate in crushing; 5. broken soil particles; 6. separated potatoes; 7. lifting chain; 8. collection device.
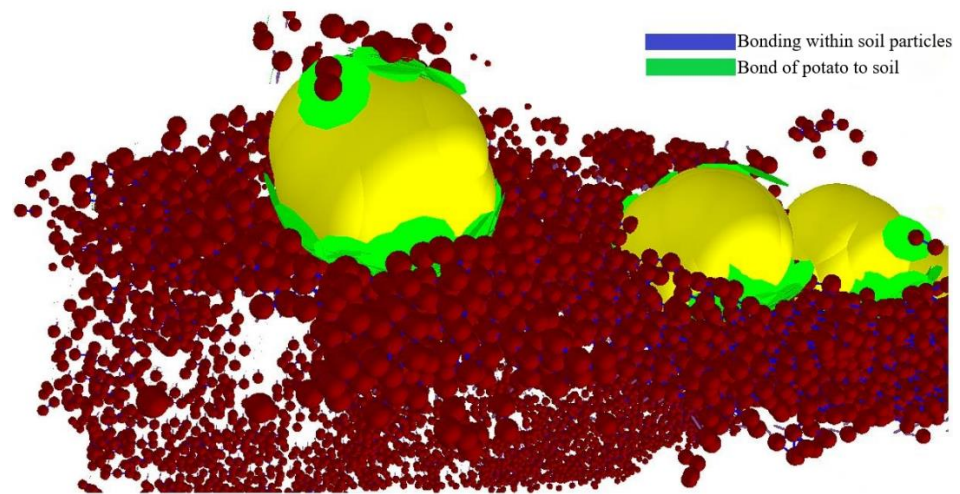
Figure 7. Potato soil agglomerates in the breakage and binding bonds.

2.2.4. The Setting of Discrete Element Simulation Parameters

When using the particle cohesion model for the simulation of potato soil agglomerates for fragmentation and separation, basic particle physical parameters (Poisson's ratio, shear model, and density), inter-particle contact parameters (recovery coefficient, static friction coefficient, and rolling friction coefficient), and soil inter-particle contact parameters need to be determined [5,6,13,36]. For the impact coefficient of restitution of materials, we tested the impact force of potato and soil through a direct impact test. The impact materials include 65Mn rods, rods covered with rubber tubes, and soil. Then, calculate the recovery factor between materials and collision materials. We tested the maximum stiction and rolling friction between potatoes and different materials through friction tests, including 65Mn rods, rods covered with rubber tubes, and rods covered with soil. Then, we tested the maximum stiction and rolling friction between the soil and the above materials. After obtaining the data, calculate the static friction coefficient and rolling friction coefficient between each material. The maximum shear stress and maximum shear stress of soil were tested with the soil accumulation angle test and direct shear test, then the EDEM simulation software was used to restore and fit the above experiments, and finally, the discrete element calibration parameters of soil were obtained. Based on previous experimental data and references from the research group, the following data were obtained. In the following three tables, Table 1 is material physical properties, Table 2 is material contact properties, and Table 3 is the parameters of linkage action between soil particles.

Table 1. Material properties.

Materials	Poisson's Ratio υ	Shear Modulus G/Pa	Density ρ/kg·m^{-3}
Potatoes	0.49	1.12×10^6	1120
65Mn	0.30	7.92×10^{10}	7650
Soil	0.30	4.62×10^5	1500
Rubber	0.47	2.67×10^6	910

Table 2. Material contact properties.

	Recovery Factor	Static Friction Coefficient	Rolling Friction Coefficient
Potato with 65Mn	0.40	0.31	0.03
Potatoes and potatoes	0.31	0.39	0.04
Potato and rubber	0.31	0.62	0.05
Soil with 65Mn	0.16	0.60	0.35
Soil and potatoes	0.06	0.50	0.01
Soil and rubber	0.10	0.80	0.50
Soil and soil	0.13	0.56	0.27

Table 3. Parameters of linkage action between soil particles.

Parameters	Numerical Value	Unit
Normal stiffness per unit area	1.7×10^8	$N \cdot m^{-3}$
Tangential stiffness per unit area	9×10^7	$N \cdot m^{-3}$
Normal critical stress	45,000	Pa
Tangential critical stress	6000	Pa

The blade motion involves two processes: one is the uniform rotation around the rotation axis with a distance of half a circle and the other is the constant translational motion upwards along the surface of the lift chain after the rotation is completed. The velocity of the translational motion is set in the motion parameters, and the rotation speed is equal to the ratio of the translational speed to the radius around the axis.

The lifting chain is in rotational motion, and the movement speed is set in the motion parameters.

The tilt angle of the crushing and separation device is the same as the tilt angle of the lift chain. By changing the direction of gravity acceleration in the environment, the tilt angle of the entire device can be adjusted.

The blade speed, lift chain bar speed, and tilt angle of the lift chain were used as the test factors, and the specific parameters were set in the subsequent tests.

2.3. Experimental Design

In the simulation analysis, the devices that directly influence the movement of potato soil agglomerates are the lower blades of the overburden rotating plate mechanism, the upper bars of the lifting chain, and the tilting angle of the lifting chain. In addition, the blade shape also affects the crushing and separation of the soil. To clarify the pattern of the effect of each factor on soil fragmentation and obtain the relationship and optimal combination of the interaction of the factors, a single-factor test and a response surface test were conducted.

2.3.1. Single-Factor Experimental Design

The single-factor test factors were blade rack type (A), lower blade speed (B), upper lift chain bar line speed (C), and lift chain tilt angle (D).

To test the effect of different blade rack types on the soil crushing impact, the triangular rack blade, rectangular rack blade, and oblique rack blade were analyzed, which were used most frequently in soil crushing and separation devices. After determining the optimal blade rack type, the single-factor simulation tests were conducted on the lift chain bar line speed, blade speed, and lift chain tilt angle using this blade rack type. When only single-factor variation was examined, the other factors were taken as the median value, i.e., the blade speed was 0.4 m/s, the line speed of the lift chain bar was 0.302 m/s, the tilt angle of the device was 45°, and the blade rack type was fixed with the optimal kind. Each group of tests was repeated three times, and the average value was taken. The different blade rack types are shown in Figure 8. The experimental design is shown in Table 4.
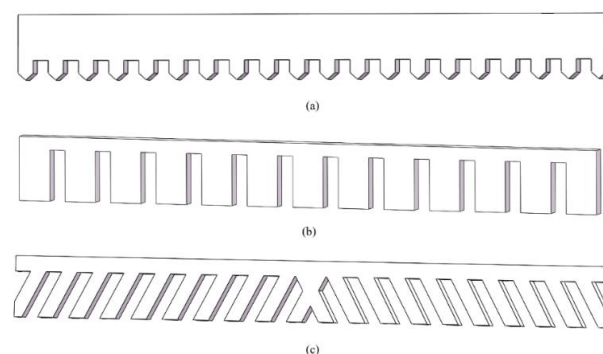

Figure 8. Comparison of blade rack types. (**a**) Triangular rack blade. (**b**)Rectangular rack blade. (**c**) Oblique rack blade.

Table 4. Single-factor test table.

Tests	Tilt Angle/°	Blade Speed/ m·s^{-1}	Lift Chain Bar Line Speed/m·s^{-1}	Blade Rack Type
1				Triangular rack blade
2	45	0.6	0.302	Rectangular rack blade
3				Oblique rack blade
4	30			
5	37.5			
6	45	0.6		
7	52.5			
8	60		0.302	Triangular rack blade
9		0.4		
10		0.5		
11	45	0.6		
12		0.7		
13		0.8		
14			0.151	
15			0.226	
16	45	0.6	0.302	
17			0.377	
18			0.453	

2.3.2. Response Surface Experimental Design

To clarify the influence of critical operating parameters on the debris removal rate and soil breaking effect and solve the optimized parameter combinations, the response surface tests were carried out with the lower blade motion speed, upper lift chain bar line speed, and lift chain tilt angle as the test factors.

The factors are coded in Table 5, and the experimental design is in Table 6.

Table 5. Experimental factor codes.

Tests	Factors		
	Tilt Angle/°	Blade Speed/m·s^{-1}	Lift Chain Bar Line Speed/m·s^{-1}
−1	30	0.4	0.151
0	45	0.6	0.302
1	60	0.8	0.453

Table 6. Response surface test design scheme.

Tests	Tilt Angle/°	Blade Speed/m·s^{-1}	Lift Chain Bar Line Speed/m·s^{-1}
1	30	0.4	0.302
2	45	0.6	0.302
3	45	0.6	0.302
4	45	0.6	0.302
5	60	0.8	0.302
6	30	0.6	0.453
7	60	0.4	0.302
8	45	0.6	0.302
9	30	0.6	0.151
10	45	0.6	0.302
11	45	0.8	0.151
12	45	0.4	0.453
13	45	0.4	0.151
14	60	0.6	0.151
15	60	0.6	0.453
16	45	0.8	0.453
17	30	0.8	0.302

2.3.3. Analysis of Experimental Evaluation Indicators

The evaluation index of the single-factor test of the blade rack type was the debris removal rate, and the evaluation indexes of other single-factor tests and response surface tests were the debris removal rate, the percentage of bond breakage between potato soil particles, and the percentage of bond breakage between soil particles.

During the simulation analysis of the soil crushing and separation, the potato soil agglomerates are crushed and separated, and the potatoes will move with the lift chain bar to the end and fall into the collection device. Some of the crushed soil particles will also fall into the collection device or outside the environment at the end of the device, becoming impurities and affecting the harvesting efficiency. Some soil particles will stick to the potato surface, and some soil particles are not entirely broken and agglomerated into larger soil clumps. Therefore, this article calculates the remaining proportion of soil particles, the proportion of bond breakage between soil particles, and the proportion of potato soil particle breakage to reflect the fragmentation of the soil. Based on the EDEM post-processing function, the number of soil particles that fell outside the environment from the collection device and the end of the device can be counted, which was the basis for calculating the debris removal rate. The unbroken bonds between soil particles or potato and soil particles were recorded when the simulation was finished, which can be used to calculate the percentage of bond breakage. Figure 9 shows the line chart of soil particles changing with simulation time (a), the line chart diagram of the number of bonding bonds between soil particles and potato particles changing with time (b), and the line chart diagram of the number of bonding bonds between soil particles changing with time (c). The green line represents the change in time, while the blue line represents the change in the selected metric.
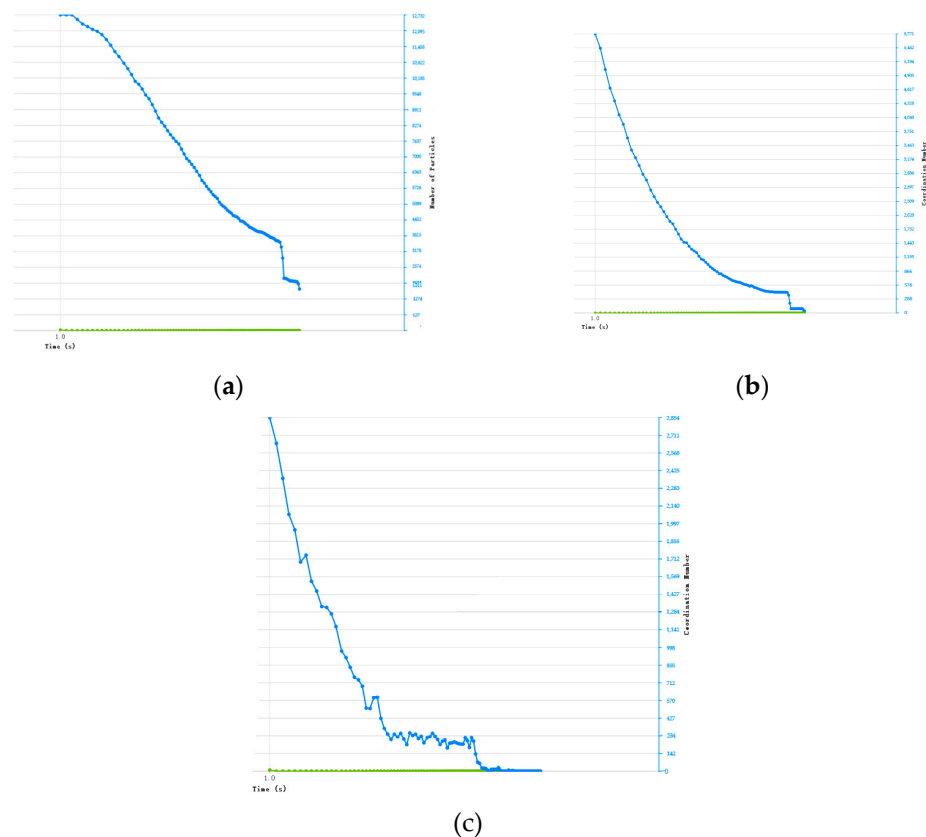

(**a**)　　　　　　　　　　　　　　　　　　　　　　　　　(**b**)

(**c**)

Figure 9. Simulation data output diagram. (**a**) Soil particles changing with time. (**b**) The number of bonding bonds between soil particles changing with time. (**c**) The number of bonding bonds between soil and potato changing with time.

3. Results

3.1. Single-Factor Test Results and Analysis

According to the simulation results of the single-factor test of blade rack type, the line graph of the effect of blade rack type on the debris removal rate is drawn. From the image, the debris removal rate of the triangular rack type is the highest, the debris removal rate of the rectangular rack type is slightly lower than the triangular rack type blade, and the debris removal rate of the oblique rack type blade is the lowest. During the simulation, it was analyzed that the teeth width of the rectangular rack is slightly more expansive, and the gap between the teeth was slightly narrower, which made some soil particles stick to the blade and caused the separation to be uncompleted. In contrast, the teeth of the oblique rack-type blade were tilted and distributed, which made some soil not pass through the gap between the teeth. Compared with the other two blades, the contact area between soil particles and the oblique rack-type blade was more extensive and easier to stick to. Hence, the debris removal rate was the lowest. The single-factor experimental results of blade type are shown in Figure 10.
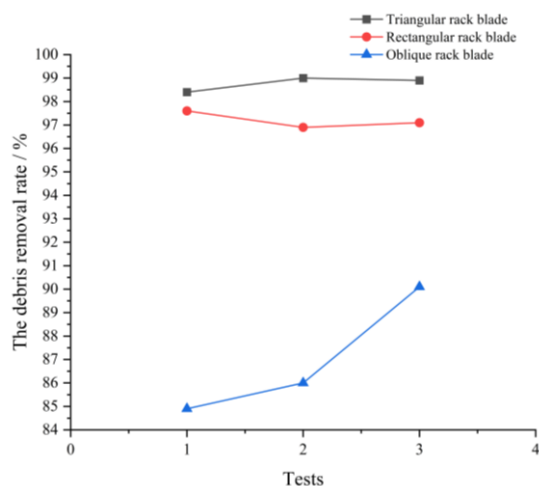

Figure 10. Single-factor test diagram of blade rack type.

Based on the simulation results of the single-factor test of the tilt angle, the line graphs of the tilt angle and the debris removal rate, the percentage of bond breakage between potato soil particles, and the percentage of bond breakage between soil particles are plotted, as shown in Figure 11. It was found that the debris removal rate and the percentage of bond breakage between soil particles decreased with the increase in the tilt angle. When the tilt angle increases from 30° to 60°, the debris removal rate drops from 98.1% to 84.4% (a fluctuation of 13.7%). The percentage of bond breakage between soil particles decreases from 99.3% to 86.7%, and the percentage of bond breakage between potato soil particles remains above 95. According to simulation process analysis, this is because as the tilt angle increases, some crushed soil particles stick to the blade and then move to the end of the lifting chain, resulting in a higher soil content and a lower percentage of debris removal rate.

According to the simulation results of the single-factor test of blade speed, the line graphs of blade speed and debris removal rate, the percentage of bond breakage between potato soil particles, and the percentage of bond breakage between soil particles are plotted, as shown in Figure 12. The debris removal rate decreases with the increase in blade speed. When the blade speed increases from 0.4 m/s to 0.6 m/s, the debris removal rate drops from 98.4% to 89.3% (a fluctuation of 9.1%). The percentage of bond breakage between soil particles increases briefly and then decreases gradually. The percentage of bond breakage between potato soil particles decreases from 100% to 92.3%, which is because when the blade speed increases, the crushing and separation time on potato soil agglomerates decrease, resulting in insufficient soil fragmentation.
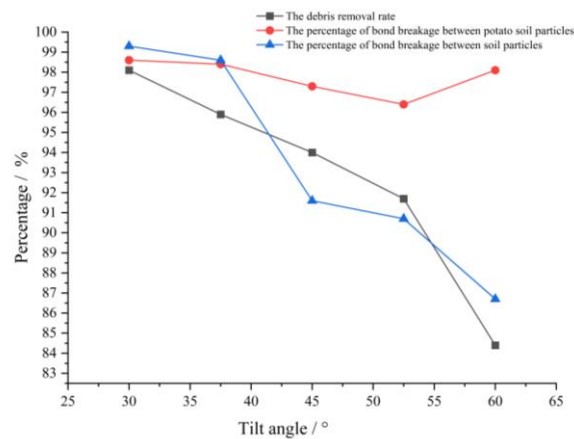
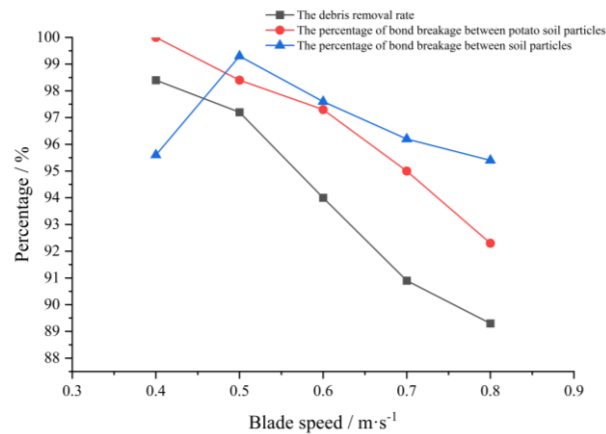**Figure 11.** Single-factor test diagram of the tilt angle.

Figure 12. Single−factor test diagram of blade speed.

According to the simulation results of the single-factor test of the lift chain bar line speed, the line graphs of the lift chain rotation speed and the debris removal rate, the percentage of bond breakage between potato soil particles, and the percentage of bond breakage between soil particles are plotted, as shown in Figure 13. The debris removal rate decreases with the increase in the linear speed of the lift chain bar. When the speed increases from 0.151 m/s to 0.453 m/s, the debris removal rate decreases from 95.6% to 92.8% (a fluctuation of 2.8%). The percentage of bond breakage between soil particles always fluctuates between 97 and 98. The percentage of bond breakage between potato soil particles decreases from 98.9 to 96, which is because when the speed of the lift chain bar increases, some soil particles will be broken and moved to the end of the lift chain before they drop from the bar gap.
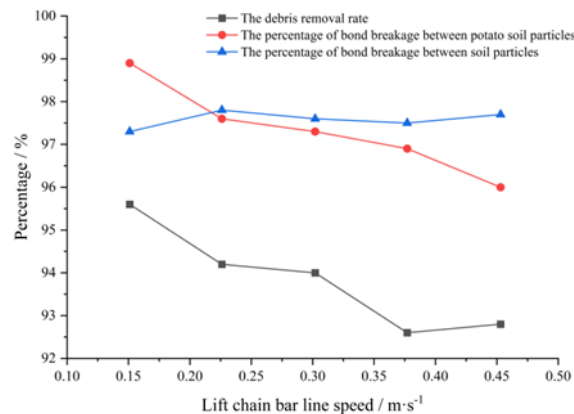

Figure 13. Single−factor test diagram of the lift chain bar line speed.

A comprehensive analysis of the above experimental results shows that reducing the tilt angle, blade speed, and lift chain bar line speed can increase the rate of debris removal and the percentage of bond breakage between potato soil particles. While with the decrease in blade speed, the percentage of bond breakage between soil particles decreases, and the effect of soil breaking is affected. Therefore, to obtain a high debris removal rate and bond breakage ratio simultaneously, multi-factor optimization tests are needed.

3.2. Response Surface Test Results and Analysis

The response surface test simulation results are shown in Table 7. The debris removal rate, the percentage of bond breakage between potato soil particles, and the percentage of bond breakage between soil particles are shown.

Table 7. Response surface test results.

Tests	Tilt Angle/ °	Blade Speed/ $m \cdot s^{-1}$	Lift Chain Bar Line Speed/ $m \cdot s^{-1}$	The Debris Removal Rate/%	The Percentage of Bond Breakage between Potato Soil Particles/%	The Percentage of Bond Breakage between Soil Particles/%
1	30	0.4	0.302	99.2	100.0	95.0
2	45	0.6	0.302	94.0	97.3	97.6
3	45	0.6	0.302	93.8	97.2	97.4
4	45	0.6	0.302	94.2	97.4	97.4
5	60	0.8	0.302	92.7	96.9	97.5
6	30	0.6	0.453	93.1	96.8	97.2
7	60	0.4	0.302	85.6	100.0	93.6
8	45	0.6	0.302	94.2	97.3	97.5
9	30	0.6	0.151	97.4	99.1	97.1
10	45	0.6	0.302	94.1	97.1	97.7
11	45	0.8	0.151	91.7	96.4	95.9
12	45	0.4	0.453	97.8	97.6	99.6
13	45	0.4	0.151	98.9	100.0	98.2
14	60	0.6	0.151	83.7	92.7	90.7
15	60	0.6	0.453	83.2	96.4	91.7
16	45	0.8	0.453	90.0	91.1	95.8
17	30	0.8	0.302	91.5	94.7	96.4

Response surface analysis of the debris removal rate and each factor.

The response surface of the effect of each factor on the debris removal rate was generated according to the model using Design-Expert 13 software. The variation of various factors on the response surface takes on a curved shape. The projection of points with the same numerical values on the response surface of each factor on the bottom surface is a continuous curve that changes with the change of another factor. The corresponding positions on the response surface when each factor reaches its extreme value correspond to the red marked points in the surface graph of the influence surface. The single-factor test shows that the impact of blade speed and tilt angle on the debris removal rate is significant, and the effect of the linear velocity of the lift chain bar on the debris removal rate is not substantial. Figure 14 shows the response surface of blade speed and tilt angle on the debris removal rate. It can be seen that with the increase in blade speed and tilt angle, the debris removal rate decreases. The main reason for this phenomenon is that the larger the blade speed, the shorter the time for soil particles to be crushed, and the time for the crushed soil particles is not enough to fall to the bottom of the lift chain; the larger the tilt angle, the easier for soil particles to re-adhesion after crushing.
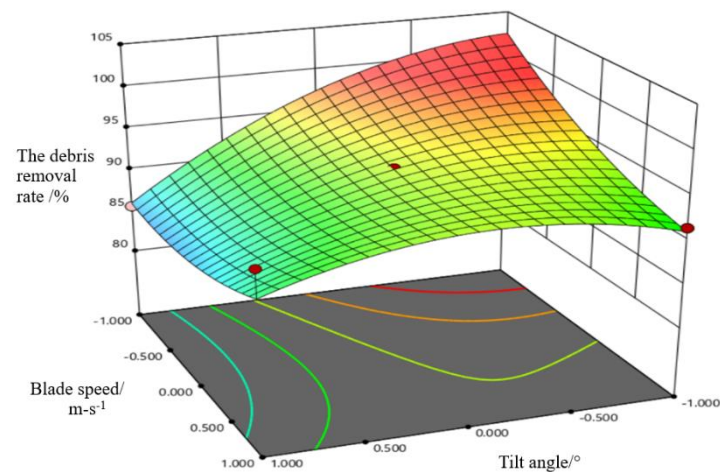
Figure 14. Response surface analysis of the percentage of bond breakage between potato soil particles and each factor.

The response surface of the effect of each factor on the percentage of bond breakage between potato soil particles is shown in Figure 15. The single-factor test shows that the effect of blade speed and lift chain bar line speed on the percentage of bond breakage between potato soil particles is significant, and the tilt angle is insignificant. It can be found that the rate of bond breakage between potato soil particles tends to decrease with the increase in blade speed and chain bar speed.
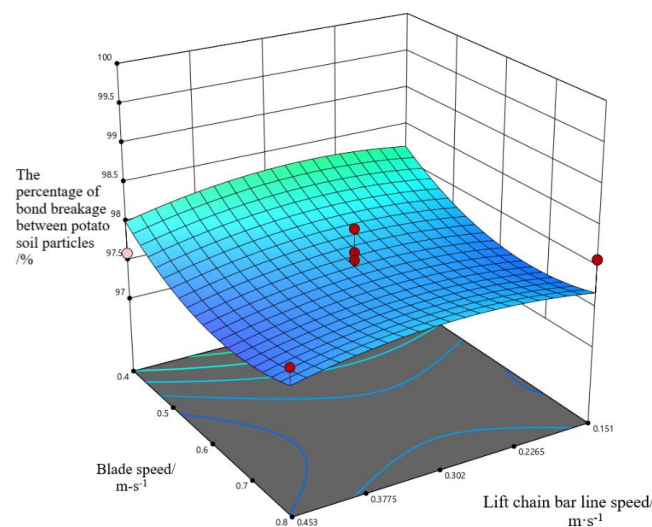

Figure 15. 10.3 Response surface analysis of the percentage of bond breakage between soil particles and each factor.

The response surface of the effect of each factor on the percentage of bond breakage between soil particles is shown in Figure 14. The single-factor test shows that the impact of blade speed and lift chain bar line speed on the percentage of bond breakage between soil particles is significant, and the tilt angle is insignificant. Based on Figure 16, it can be found that the ratio of bond breakage between soil particles tends to increase with the increase in blade speed and the line speed of the lift chain bar.
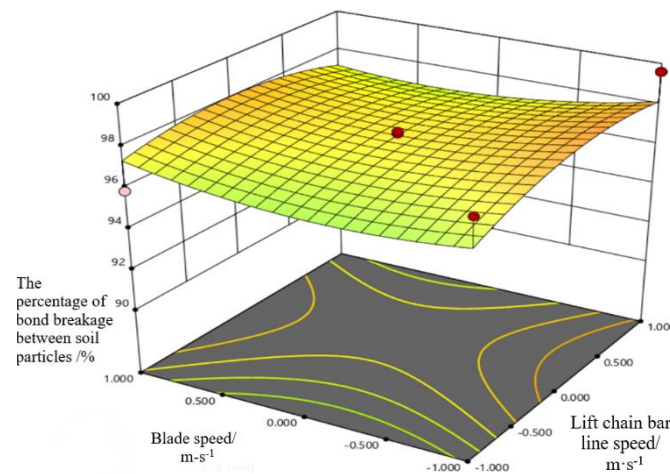
Figure 16. Response surface of the effect of interaction between blade speed and lift chain bar line speed on the percentage of bond breakage between soil particles.

3.3. Parameter Optimization and Validation

According to the results of the response surface analysis, the parameters were optimized by using the optimization function of Design-Expert 13 software. To improve production efficiency, the debris removal rate was first optimized, and the bond breakage ratio was maximized simultaneously. On this basis, the optimization model was established, and the optimal solution was found to be 0.307 m/s for the lift chain bar line speed, 0.4 m/s for the blade speed, and 40° for the tilt angle. The optimized debris removal rate was 100%, the percentage of bond breakage between potato soil particles was 99.6%, and the percentage of bond breakage between soil particles was 99.7%.

To verify the effect of each factor on the debris removal rate, the optimal solution parameters were imported into the simulation model, and the validation test was repeated three times with the test indexes of debris removal rate, the percentage of bond breakage between potato soil particles, and the percentage of bond breakage between soil particles. The levels of each factor and the validation results are shown in Table 8.

Table 8. Validation results of the simulation test.

Tests	Tilt Angle/ °	Blade Speed/m·s^{-1}	Lift Chain Bar Line Speed/ m·s^{-1}	The Debris Removal Rate/%	The Percentage of Bond Breakage between Potato Soil Particles/%	The Percentage of Bond Breakage between Soil Particles/%
1				98.9	100.0	100.0
2	40	0.4	0.307	99.4	99.6	99.7
3				99.1	98.5	99.6

The relative errors between the simulation test and model optimization values were less than 5%, which indicated that the model in this study was reliable.

4. Conclusions

The potato soil aggregate particle model and the overburden rotating plate mechanism model were constructed. The effects of blade rack types, blade speed, lifting chain bar line speed, and device inclination angle on the crushing of soil aggregates were studied, and the tilt angle of the overburden rotating plate mechanism was obtained by taking the debris removal rate, the percentage of bond breakage between potato soil particles, and the percentage of bond breakage between soil particles as evaluation indexes. Specific conclusions are as follows:

(1) Different models of potato soil agglomerates using particle bonding models provide a new method to study the fragmentation and separation of potato and soil;

(2) Design-Expert was used to construct response surfaces for the potato soil agglomerate separation rate, the soil particle breakage ratio, and the soil particle bond breakage ratio. The relationships between blade speed, lift chain bar line speed, tilt angle, debris removal rate, the percentage of bond breakage between potato soil particles, and the percentage of bond breakage between soil particles were obtained;

(3) The optimum parameters of the overburden rotating plate mechanism were verified through tests to be 0.307 m/s for the lift chain bar line speed, 0.4 m/s for the blade speed, and 40° for the tilt angle.

Author Contributions: D.Y.: conceptualization, methodology, investigation, writing—original draft preparation, and visualization. W.D.: methodology, resources, writing—review and editing, supervision, and funding acquisition. S.X.: methodology and resources. C.L.: investigation and data curation. Z.R.: project administration. H.Z.: data curation. Y.C.: data curation. Z.Z.: project administration. All authors have read and agreed to the published version of the manuscript.

Institutional Review Board Statement: Not applicable.

Informed Consent Statement: Not applicable.

Data Availability Statement: Data are contained within the article. All the code generated or used during this study is available from the corresponding author.

Conflicts of Interest: The authors declare no conflict of interest.

References

1. Wei, Z.; Su, G.; Li, X.; Wang, X.; Sun, F.; Meng, P. Parameter Optimization and Test of Potato Harvester Wavy Sieve Based on EDEM. *J. Agric. Mach.* **2020**, *51*, 109–122.
2. Wen, M. Design and Test of Seed Arrangement Device of Conveyor Belt Potato Planter. Master's Thesis, Sichuan Agricultural University, Ya'an, China, 2021.
3. Sun, H. Design and Experimental Research on Transporting and Separating Device of Lifting Chain Potato Digger. Master's Thesis, Northeast Agricultural University, Harbin, China, 2019.
4. Zhang, Z. Experimental Study and Simulation Analysis on Vibration Damage of Potato during Transportation. Master's Thesis, Inner Mongolia Agricultural University, Hohhot, China, 2022.
5. Wang, Y. Simulation Analysis and Experimental Study on Acceleration Characteristics of Potato in Potato Soil Separation Unit. Master's Thesis, Inner Mongolia Agricultural University, Hohhot, China, 2022.
6. Li, P. Development and Performance Test of Three-Stage Six-Boom Swing Separation Sieve. Master's Thesis, Inner Mongolia Agricultural University, Hohhot, China, 2022.
7. Wei, M. The Design and Simulation Analysis of Key Components of the Roller Potato Harvester. Master's Thesis, Hubei University of Technology, Wuhan, China, 2018.
8. Yang, R.; Yang, H.; Shang, S.; Ni, Z.; Liu, Z.; Guo, D. Design and Experiment of Vertical Circular Separating and Conveying Device for Potato Combine Harvester. *Trans. Chin. Soc. Agric. Eng.* **2018**, *34*, 10–18.
9. Zi, Z.; Jin, J.; Chang, Z.; Qun, Y.; Xiu, S. Design and Experimental Study on The Conveying Chain Soil Cleaning Device of Potato Harvester. *J. Agric. Mech. Res.* **2016**, *2*, 123–127.
10. Hu, G. *Discrete Element Method Analysis and Simulation of Particle System: Industrial Application of Discrete Element Method and Introduction to EDEM Software*; Wuhan University of Technology Press: Wuhan, China, 2010.
11. Cundalll, P.A. A discrete numerical model for granular assemblies. *Geotechnique* **1979**, *29*, 47–65. [CrossRef]
12. Huang, W. Parameter calibration of discrete element model for sandy soil particles. *Fujian Build. Mater.* **2023**, *2*, 1–5.
13. Li, J.; Xie, S.; Liu, F.; Guo, Y.; Liu, C.; Shang, Z.; Zhao, X. Calibration and Testing of Discrete Element Simulation Parameters for Sandy Soils in Potato Growing Areas. *Appl. Sci.* **2022**, *12*, 10125. [CrossRef]
14. Jiang, Y.; Hong, Y.; Ni, J. Micro-Investigation of Shear Strength of Sand Based on Discrete Element Method. *Low Temp. Constr. Technol.* **2022**, *44*, 96–101.

15. Alfaris Murtadha, A.; Almaliki Salim, A. Effect of Tillage Depth and Lateral Distance of Shallow Plows on the Mean Weight Diameter and the Energy of Soil Fragmentation by Using Locally Manufactured Subsoiler Plow. *IOP Conf. Ser. Earth Environ. Sci* **2022**, *1060*, 012129. [CrossRef]

16. Tagar, A.A.; Adamowski, J.; Memon, M.S.; Do, M.C.; Mashori, A.S.; Soomro, A.S.; Bhayo, W.A. Soil fragmentation and aggregate stability as affected by conventional tillage implements and relations with fractal dimensions. *Soil Tillage Res.* **2020**, *197*, 104494. [CrossRef]

17. da Silva Martinez, A.; Seidel, E.P.; Pan, R.; Brito, T.S.; Meiners, W. Crop rotation and soil scarification: Impacts in the soil penetration resistance. *Commun. Plant Sci.* **2019**, *10*, 26814.

18. Zhao, B.; Men, L.; Song, L.; Wang, Y.; Ye, J.; Jiang, H.; Liu, Y.; Luo, J.; Guo, J.; Guo, X. Mechanical properties analysis and experiment on Multi-order excavation shovel of Ophiopogon japonicas harvester. *J. Phys. Conf. Ser.* **2021**, *1986*, 012016. [CrossRef]

19. Li, Y.; Fan, J.; Hu, Z.; Luo, W.; Yang, H.; Shi, L.; Wu, F. Calibration of Discrete Element Model Parameters of Soil around Tubers during Potato Harvesting Period. *Agriculture* **2022**, *12*, 1475. [CrossRef]

20. Chen, L.; Xue, J. Research on the calibration method of cassava seed stem simulation parameters based on discrete elements. *Jiangsu Agric. Sci.* **2023**, *51*, 198–205.

21. Liu, Y.; Zhao, J. Parameters calibration of discrete element of clay soil in yam planting area. *J. Hebei Agric. Univ.* **2021**, *44*, 99–105.

22. Liu, Y. Model Construction of Root—Soil Complex of Yam and Experimental Study on de—Soiling. Master's Thesis, Hebei Agricultural University, Baoding, China, 2021.

23. Liu, W.; He, J. Calibration of Simulation Parameters for Potato Minituber Based on EDEM. *Trans. Chin. Soc. Agric. Mach.* **2018**, *49*, 125–135+142.

24. Liu, G. Experimental Study on Potato Motion Characteristics during Potato Soil Separation Process. Master's Thesis, Inner Mongolia Agricultural University, Hohhot, China, 2022.

25. Zhang, Q. Analysis of Potato Collision Problem and Research and Development of Key Components of Separator Based on Discrete Element. Master's Thesis, Shandong University of Science and Technology, Zibo, China, 2022.

26. Song, Z.; Li, H.; Yan, Y. Calibration Method of Contact Characteristic Parameters of Soil in Mulberry Field Based on Unequal-diameter Particles DEM Theory. *Trans. Chin. Soc. Agric. Mach.* **2022**, *53*, 21–33.

27. Wu, T.; Huang, W.; Chen, X.; Ma, X.; Han, Z.; Pan, T. Calibration of discrete element model parameters for cohesive soil considering the cohesion between particles. *J. South China Agric. Univ.* **2017**, *38*, 93–98.

28. Tao, L.; Shi, Y.; Huang, L.; Lin, S.; Liu, Y.; Li, X. Parameter Calibration of Soil Discrete Element Simulation Model for Sugarcane Cultivation in Guangxi Coastal Area. *Acta Agric. Jiangxi* **2022**, *34*, 94–100.

29. Yu, C. Study on the Failure Mechanism of High Slope of Soil Roadbed Based on Particle Discrete Element Method. *Traffic Eng. Technol. Natl. Def.* **2022**, *20*, 19–22.

30. Fan, W.; Zhang, F.; Yan, J.; Zheng, L.; Pan, D.; Han, Z. Discrete element simulation calibration and testing of the interaction between clay and loose soil components. *J. Agric. Mech. Res.* **2024**, *46*, 177–182+190.

31. Zhang, C.; Hu, X.; Liu, J.; Yang, Y.; Li, Y. Calibration and Verification of Bonding Parameters of Banana Straw Simulation Model Based on Discrete Element Method. *Trans. Chin. Soc. Agric. Mach.* **2023**, *54*, 121–130.

32. Li, Q.; Zheng, X.; Liu, J.; Yang, H.; Wang, Z.; Zhang, L. Calibration of Discrete Element Simulation Parameters for Farmland Silt in Xinjiang. *Xinjiang Agric. Sci.* **2022**, *59*, 2014–2024.

33. Zhang, S.; Zhou, J.; Liu, H.; Shi, S.; Wei, G.; He, T. Determination of Interspecific Contact Parameters of Corner Simulation Calibration of Discrete Element. *Trans. Chin. Soc. Agric. Mach.* **2022**, *53*, 69–77.

34. Meng, J.; Wang, C. Modeling and motion simulation analysis of potato based on 3D scanning. *J. Agric. Mech. Res.* **2015**, *37*, 64–67.

35. Ucgul, M.; Fielke, J.M.; Saunders, C. Three dimensional discrete element modeling DEM of tillage accounting for soil cohesion and adhesion. *Biosyst. Eng.* **2015**, *129*, 298–306. [CrossRef]

36. Deng, W. Study on the Collision Damage Characteristics and Peel Friction Damage Mechanisms of Potato Tubers. Doctor's Thesis, Inner Mongolia Agricultural University, Hohhot, China, 2022.